Investigations on the mixed Jahn-Teller system (Tb_x, Dy_{1-x})VO_4. III. Birefringence measurements in the monoclinic phase

1990 J. Phys.: Condens. Matter 2 1113

(http://iopscience.iop.org/0953-8984/2/5/005)

J. Phys.: Condens. Matter **2** (1990) 1113–1120. Printed in the UK

Investigations on the mixed Jahn–Teller system $(Tb_x,Dy_{1-x})VO_4$: III. Birefringence measurements in the monoclinic phase

G Hess, W Hikel and H G Kahle
Physikalisches Institut, Universität Karlsruhe (TH), PO Box 6980, D-7500 Karlsruhe 1, Federal Republic of Germany

Received 2 May 1989, in final form 22 August 1989

Abstract. Birefringence measurements on the mixed crystal system $(Tb_x,Dy_{1-x})VO_4$ at different wavelengths in the visible part of the spectrum prove the macroscopic superposition of the two distortion types of Jahn–Teller-active $TbVO_4$ and $DyVO_4$ for concentrations $0.35 \leqslant x \leqslant 0.45$. Because of the superposition of the distortion types the crystals become monoclinic at low temperatures.

1. Introduction

In the first paper of this series [1], henceforth referred to as I, we reported on the phase diagram of the mixed Jahn–Teller system $(Tb_x,Dy_{1-x})VO_4$ (figure 1 of paper I). For concentrations $x \leqslant 0.3$ the crystals distort like pure $DyVO_4$, which lowers its tetragonal high-temperature structure by a Γ_4^+ distortion, i.e. the square base of the unit cell becomes a rectangle. For $x \geqslant 0.45$ the crystals distort like pure $TbVO_4$, which lowers its symmetry by a Γ_3^+ distortion, i.e. the square base of the unit cell becomes a rhomb. For $x = 0.35$, $x = 0.40$ and in finite magnetic fields for $x = 0.45$, the two distortion types superimpose. This means that at $T = T_{D1}$ the crystals become Γ_3^+ distorted and at $T = T_{D2} < T_{D1}$ they additionally become Γ_4^+ distorted. They are then monoclinic and a dispersion of the optical indicatrix axes is observed (paper I).

In the second paper [2], henceforth referred to as II, we presented studies of the linear optical birefringence for the two orthorhombic phases. In the present paper we discuss the consequences of the superposition of the two types of distortion for the birefringence. We further show that the observed birefringence curves in this phase are caused by the simultaneous presence of the two distortions.

2. Experimental details

The low-temperature set-up and the light sources used in the experiments were the same as in paper II. The birefringence was measured by using light modulation (50 kHz) and computer-controlled compensation of the corresponding phase difference through a

0953-8984/90/051113 + 08 $03.50

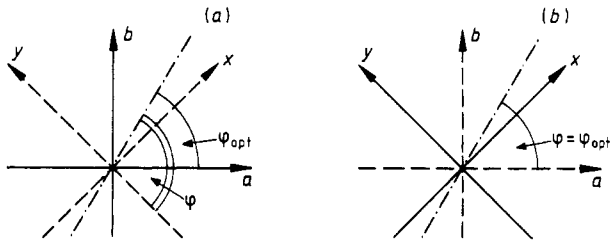

Figure 1. Set-up of the optical components. The axes are defined in terms of the undistorted tetragonal crystal system as $\boldsymbol{a} \equiv [1,0,0]$, $\boldsymbol{b} \equiv [0,1,0]$, $\boldsymbol{x} \equiv [1,1,0]$ and $\boldsymbol{y} \equiv [1,\bar{1},0]$. The light propagates along $\boldsymbol{c} \equiv [0,0,1]$. Full lines: transmission direction of polariser and analyser. Broken lines: directions of the azimuths of modulator and compensator, thus being at $\pi/4$ with respect to the transmission direction of the polariser. Chain line: direction of one of the principal refractive indices of the sample; φ_{opt} is the angle between the latter direction and the $\boldsymbol{a}$ axis. (*a*) Set-up I, generally used for measuring δn_X; in this case $\varphi = \varphi_{opt} + \pi/4$. (*b*) Set-up II, generally used for measuring δn_A; in this case $\varphi = \varphi_{opt}$.

compensator. Two optical set-ups were used (see figure 1). In set-up I the transmission direction of the polariser is along $\boldsymbol{a}$ or $\boldsymbol{b}$, the azimuths of modulator and compensator at $\pi/4$ with respect to $\boldsymbol{a}$ and $\boldsymbol{b}$ (figure 1(*a*)). This set-up was used to measure the birefringence δn_X in the orthorhombic case (see paper II) and it was also generally used for measuring δn_X in the monoclinic case. In set-up II the optical components (polariser, modulator, compensator and analyser) are turned by $\pi/4$ with respect to set-up I, but the sample is left in its position (figure 1(*b*)). This set-up was used to measure the birefringence δn_A. To avoid crystallographic domains a small magnetic field was applied. Three different field directions with respect to the crystal axes were used: (i) parallel to $\boldsymbol{a}$, in which case no Γ_4^+ domains exist but Γ_3^+ domains are present, however; (ii) parallel to $\boldsymbol{x}$, in which case no Γ_3^+ domains exist but Γ_4^+ domains are present; (iii) parallel to $\boldsymbol{w}$ with $\boldsymbol{w}$ = bisectrix of $\boldsymbol{a}$ and $\boldsymbol{x}$, i.e. $\sphericalangle(\boldsymbol{a}, \boldsymbol{w}) = \sphericalangle(\boldsymbol{w}, \boldsymbol{x}) = \pi/8$, in which case neither Γ_3^+ domains nor Γ_4^+ domains exist.

3. Birefringence in monoclinic crystals

3.1. Monoclinic distortion

In paper I the distortions of the pure substances $DyVO_4$ and $TbVO_4$ were written as

$$e_A = 2e_{11} = e_{11} - e_{22} = \Delta a/a - \Delta b/b \tag{1}$$

for the Γ_4^+ distorted $DyVO_4$ and

$$e_X = 2e_{12} = \Delta x/x - \Delta y/y \tag{2}$$

for the Γ_3^+ distorted $TbVO_4$. Here e_{11}, e_{121}, e_{22} are components of the strain tensor [3], $\boldsymbol{a}$, $\boldsymbol{b}$ are the tetragonal [1,0,0] and [0,1,0] directions and $\boldsymbol{x}$, $\boldsymbol{y}$ are the tetragonal [1,1,0] and [1,$\bar{1}$,0] directions, respectively.

The strain tensor for a superposition of the two distortion types then reads

$$\boldsymbol{e} = \begin{pmatrix} e_{11} & e_{12} \\ e_{12} & -e_{11} \end{pmatrix} = \tfrac{1}{2}\begin{pmatrix} e_A & e_X \\ e_X & -e_A \end{pmatrix} \tag{3}$$

where the third components are omitted. The difference of the eigenvalues of the tensor $\boldsymbol{e}$

$$\lambda_1 - \lambda_2 = (e_A^2 + e_X^2)^{1/2} \tag{4}$$

gives the distortion in a direction tilted by the angle φ_{elast} off the $[1,0,0]_{tetr}$ direction with

$$\tan(2\varphi_{elast}) = e_A/e_X. \tag{5}$$

3.2. *Monoclinic birefringence*

In the orthorhombic phases where either $e_X = 0$ or $e_A = 0$, the distortions e_A and e_X, respectively, cause a birefringence $\delta n(\lambda)$ (λ = wavelength of the light), whose dependence on the distortions is written as

$$\delta n_A(\lambda) = f_A(\lambda, e_A) \tag{6}$$

for the Γ_4^+ distorted crystals and

$$\delta n_X(\lambda) = f_X(\lambda, e_X) \tag{7}$$

for the Γ_3^+ distorted crystals. Here δn_A or δn_X are the differences of the principal refractive indices. In the simplest case the functions f_A and f_X are linear in e_A and e_X, respectively.

In the monoclinic phase, both e_A and e_X are different from zero. Using Maxwell's and the material equations one gets the eigenvalue equation for n^{-2} (see, e.g. [4])

$$(n^{-2}\delta_{\alpha\beta} - B_{\alpha\beta})D_\beta = 0 \tag{8}$$

where α, $\beta = 1, 2$ denote the coordinates perpendicular to the wave normal, δ the Kronecker symbol, B the reciprocal permittivity tensor and D the electric displacement. Because of symmetry reasons, the elements of the tensor B in the monoclinic phase ($B_{\alpha\beta}$) are connected with those in the tetragonal phase (B_{11}^0) by $B_{11} = B_{11}^0 + \Delta B_{11}$, $B_{22} = B_{11}^0 - \Delta B_{11}$, $B_{12} = \Delta B_{12}$. Assuming ΔB_{11} and ΔB_{12} to be small compared with B_{11}^0, the difference of the principal refractive indices is given by

$$\delta n = n_1 - n_2 = -n_0^3[(\Delta B_{11})^2 + (\Delta B_{12})^2]^{1/2} \tag{9}$$

with $n_0 = 1/(B_{11}^0)^{1/2}$ the refractive index of the undistorted tetragonal phase. In the two orthorhombic phases with either $\Delta B_{12} = 0$ or $\Delta B_{11} = 0$, δn equals the birefringences δn_A or δn_X, respectively, i.e.

$$\begin{aligned} \delta n_A &= -n_0^3\,\Delta B_{11} \\ \delta n_X &= -n_0^3\,\Delta B_{12}. \end{aligned} \tag{10}$$

Using these equations, one gets the expression for the monoclinic phase

$$\delta n(\lambda) = [\delta n_A^2(\lambda) + \delta n_X^2(\lambda)]^{1/2}. \tag{11}$$

While in the two orthorhombic phases δn_A and δn_X, respectively, are differences of principal refractive indices, this meaning is lost in the monoclinic phase.

The direction of the azimuth φ_{opt} (the angle between the direction of one of the principal refractive indices and the *a* axis; see figure 1) corresponds to the direction of an eigenvector of equation (8) which is given by

$$\tan[2\varphi_{opt}(\lambda)] = \delta n_X(\lambda)/\delta n_A(\lambda). \tag{12}$$

To study the dependence of the birefringence on the distortion, δn_A and δn_X (and not δn and φ_{opt}) are the quantities directly depending on the distortion of the crystal.

3.3. Measurement of monoclinic birefringence

Several more or less expansive techniques for the measurement of the monoclinic birefringence have been published [5–7]. In these techniques δn and φ_{opt} are measured. In principle δn_A and δn_X could be determined through the inversion of equations (11) and (12). None of these techniques was suitable in our case, however, since the cryostat windows had a relatively high birefringence, which even depended on the locus of the penetration and caused errors especially for $\varphi_{opt} \simeq \pi/4$. Detailed calculations proved that an arrangement in which δn_A and δn_X are measured directly is less sensitive to the errors introduced by the unknown birefringence of the windows. Therefore the set-ups described in § 2 were used.

Applying Jones' calculus for the optical components [8], the compensator phase σ_C to produce zero intensity of the modulation frequency at the detector is given by

$$\tan\sigma_C = \frac{-\sin\sigma\cos(2\varphi)}{\cos^2(2\varphi)\cos\sigma + \sin^2(2\varphi)} \tag{13}$$

where $\sigma = \delta n 2\pi d/\lambda$ (d = thickness of the crystal), $\varphi = \varphi_{opt} + \pi/4$ for set-up I and $\varphi = \varphi_{opt}$ for set-up II, respectively (see figure 1). σ_C is transformed to the apparent birefringence δn_{app} through $\delta n_{app} = \sigma_C\lambda/2\pi d$. Substituting equations (11) and (12) and the above relations into equation (13), leads to the formulae

$$\delta n_{app} = \frac{\lambda}{2\pi d}\tan^{-1}\left(\frac{\delta n_X(\delta n_X^2 + \delta n_A^2)^{1/2}\sin[(2\pi d/\lambda)(\delta n_X^2 + \delta n_A^2)^{1/2}]}{\delta n_A^2 + \delta n_X^2\cos[(2\pi d/\lambda)(\delta n_X^2 + \delta n_A^2)^{1/2}]}\right) + \frac{N\lambda}{2d} \tag{14}$$

for set-up I and

$$\delta n_{app} = \frac{\lambda}{2\pi d}\tan^{-1}\left(\frac{-\delta n_A(\delta n_X^2 + \delta n_A^2)^{1/2}\sin[(2\pi d/\lambda)(\delta n_X^2 + \delta n_A^2)^{1/2}]}{\delta n_X^2 + \delta n_A^2\cos[(2\pi d/\lambda)(\delta n_X^2 + \delta n_A^2)^{1/2}]}\right) + \frac{N\lambda}{2d} \tag{15}$$

for set-up II, respectively, where the integer N is due to the ambiguity of the $\tan^{-1}$ function. In these equations the unknown birefringence of the cryostat windows is not taken into account. As the calculations showed its consideration would change the results of the measurements only slightly.

For the following limits equations (14) and (15) can be simplified:

(i) Both birefringences, δn_A and δn_X, are small with $[(2\pi d/\lambda)(\delta n_X^2 + \delta n_A^2)^{1/2}] \ll \pi/2$. Then $\delta n_{app} = \delta n_X$, measured in set-up I, and $\delta n_{app} = \delta n_A$, measured in set-up II, respectively. That means that both birefringences are correctly measured.

(ii) One of the birefringences is small and small compared to the other, e.g. $|\delta n_X| \ll |\delta n_A|$ and $\delta n_X \ll \pi/2$. Then with equation (15), the greater birefringence, δn_A, is correctly measured, but the smaller one, δn_X, cannot be determined at all.

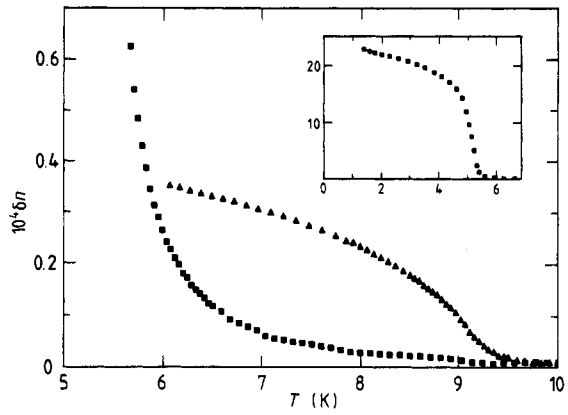

Figure 2. Measured birefringence of $(Tb_{0.4},Dy_{0.6})VO_4$ as a function of temperature around the phase transitions at T_{D1} and T_{D2}, $\lambda = 691$ nm. Squares: δn_A, $\boldsymbol{B}\|\boldsymbol{a}$ ($B = 0.03$ T). Triangles: $-\delta n_X$, $\boldsymbol{B}\|\boldsymbol{x}$ ($B = 0.05$ T). Inset: δn_A in the low-temperature region. To avoid overlap not all experimental points are shown in this and the following figures.

4. Experimental results and discussion

The limits discussed at the end of the last section are realised for some temperature and wavelength regions.

The δn_A birefringence is correctly measured for the crystals $(Tb_{0.35},Dy_{0.65})VO_4$ and $(Tb_{0.4},Dy_{0.6})VO_4$ in the green, yellow and red parts of the spectrum, for $T < T_{D2}$. The reason is that $|\delta n_X|$ is very small in this spectral range because of the compensation of different contributions to the birefringence (see paper II). In figure 2 the temperature dependence of δn_A (measured in set-up II, in a magnetic field $\boldsymbol{B}\|\boldsymbol{a}$) and that of δn_X (measured in set-up I, in a magnetic field $\boldsymbol{B}\|\boldsymbol{x}$) are compared for $(Tb_{0.4},Dy_{0.6})VO_4$ at $\lambda = 691$ nm. For $T_{D2} < T < T_{D1}$ both δn_A and δn_X are small and the limit (i) is realised. For $T < T_{D2}$, δn_A is increased to such values that the limit (ii) is realised. In this temperature region the birefringence δn_X cannot then be ascertained.

In figure 3 measurements on $(Tb_{0.35},Dy_{0.65})VO_4$ at $\lambda = 436$ nm are presented. Figure 3(a) shows δn_A measured in set-up II with $\boldsymbol{B}\|\boldsymbol{a}$ together with a calculation for a Γ_4^+ distortion on the basis of the theoretical model developed in paper II for the orthorhombic case. Although in the orthorhombic symmetry with Γ_3^+ distortion the δn_X birefringence changes by orders of magnitude over the visible part of the spectrum, the δn_A curves measured on this sample for different wavelengths are proportional to each other to a very good approximation. Thus the agreement between measurements and calculations is very good for all wavelengths. Figure 3(b) shows δn_X measured in set-up I with $\boldsymbol{B}\|\boldsymbol{x}$ together with the calculation for a Γ_3^+ distortion by means of the theoretical model developed in II. Again there is very good agreement for the temperature region $T_{D2} < T < T_{D1}$. The deviations between the measurements and the calculation for $T < T_{D2}$ are a clear indication of the occurrence of an additional Γ_4^+ distortion, leading to a lowering of the crystal symmetry to monoclinic. The parameters used for the calculations of the order parameters e_A and e_X are given in table 3 of paper I, and the connection with the birefringence shown in figures 3(a) and (b) is established via equations (14) and (16) of paper II using the parameters given in table 3 of II.

For a magnetic field $\boldsymbol{B}\|\boldsymbol{w}$, in set-up II, the situation is quite different. No Γ_3^+ domains are present in this case (see paper I) and the δn_X birefringence affects the measurement of δn_A. The measured curve (figure 3(a) and the enlargement of the region around $T \simeq 6.5$ K, figure 3(d)) differs distinctly from the δn_A curve shown in figure 3(a). The

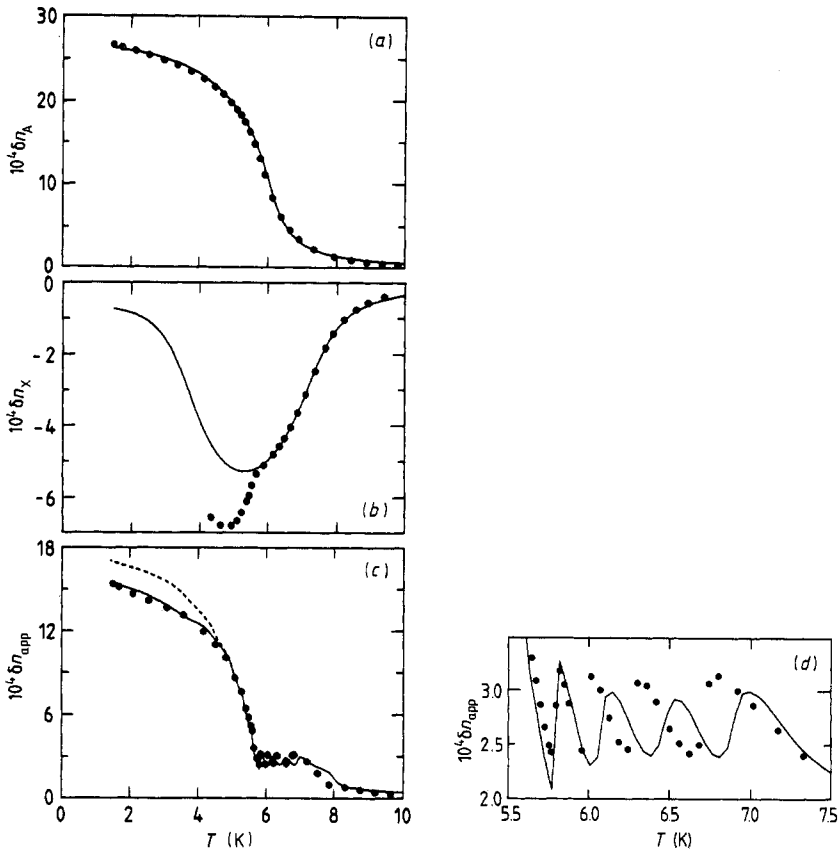

Figure 3. Measured birefringence of $(Tb_{0.35},Dy_{0.65})VO_4$, $\lambda = 436$ nm (dots) compared with theoretical curves (full curves). (*a*) δn_A, $\boldsymbol{B} \| \boldsymbol{a}$ ($B = 0.15$ T), curve calculated according to equation (17) of paper II. (*b*) δn_X, $\boldsymbol{B} \| \boldsymbol{x}$ ($B = 0.15$ T), curve calculated according to equation (15) of paper II. (*c*) Birefringence δn_{app}, measured in set-up II, $\boldsymbol{B} \| \boldsymbol{w}$ ($B = 0.15$ T). Full curve: calculated according to equation (12) of this paper using the calculated δn_A and δn_X values of (*a*) and (*b*). Broken curve: calculated assuming δn_X to be constant for $T \leqslant 5.3$ K. (*d*) Enlargement of (*c*) around $T \simeq 6.5$ K.

apparent birefringence curve in this case is well explained by a superposition of the intrinsic δn_A and δn_X according to equation (15). The values of δn_A and δn_X were taken from the calculations of figures 3(*a*) and (*b*). Both the number and the amplitude of the strange oscillations for $5.5\ \text{K} < T < 7.5\ \text{K}$ are correctly reproduced. Inspection of equation (15) shows that these oscillations occur if $|\delta n_A| < |\delta n_X|$ and if simultaneously the argument of the sine function in the numerator of equation (15) varies by more than 2π. The exact position of the oscillations differs somewhat for calculation and measurement. This does not question the validity of equation (15), but can be explained with inaccuracies in the temperature measurements. In the same way, the apparent birefringence is qualitatively well reproduced for $T < T_{D2}$. It is sensitive to changed values of δn_X, as is shown by a comparison of the different calculations in figure 3(*c*). The full curve is calculated using δn_X as shown by the full curve in figure 3(*b*), the broken curve using the minimum of the calculated δn_X (at $T = 5.3$ K) as a fixed value. Although

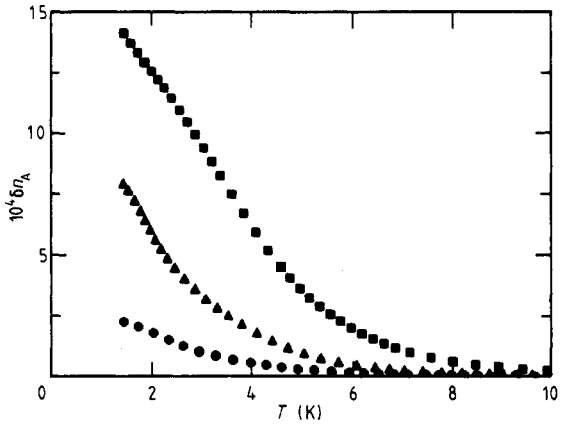

Figure 4. Measured temperature dependence of the birefringence δn_A of $(Tb_{0.45},Dy_{0.55})VO_4$ for different external fields $\boldsymbol{B}\|\boldsymbol{a}$, λ = 633 nm: ●, B = 0.05 T; ▲, B = 0.10 T; ■, B = 0.15 T.

therefore the course of δn_X for $T < T_{D2}$ cannot be deduced exactly from the measurement of the apparent birefringence, it is not in contradiction to the assumed mean-field behaviour. This leads to the conclusion that within the measuring accuracy the distortions e_A and e_X responsible for the corresponding intrinsic birefringences δn_A and δn_X do not affect each other. Irrespective of this, δn_A in the monoclinic phase depends in some way on e_X because the Tb contribution to δn_A depends on its occupation numbers and thus on e_X(see paper II).

For $(Tb_{0.4},Dy_{0.6})VO_4$ and $(Tb_{0.45},Dy_{0.55})VO_4$ the apparent birefringence curves can be explained in the same way by the superposition of the intrinsic δn_A and δn_X curves. For $(Tb_{0.45},Dy_{0.55})VO_4$ (and also for the crystals with a higher Tb^{3+} content) no Γ_4^+ phase transition exists. Despite this, in finite magnetic fields a strong intrinsic δn_A birefringence is observed (corresponding to the high-temperature tail of the birefringence for the crystals with phase transition). In figure 4 this is shown for different

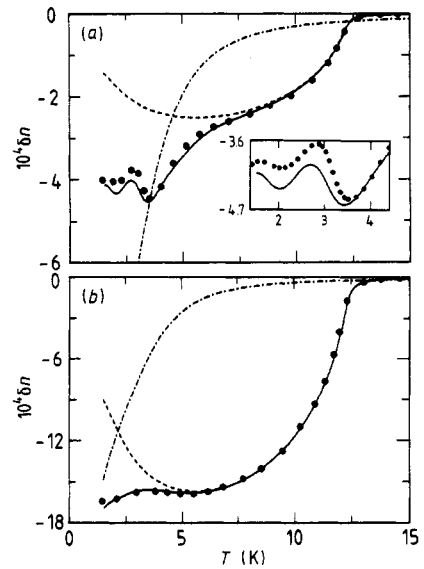

Figure 5. Birefringence δn_{app} of $(Tb_{0.45},Dy_{0.55})VO_4$, measured in set-up I with $\boldsymbol{B}\|\boldsymbol{w}$ (B = 0.15 T), compared with a calculation according to equation (11) (full curve) using the intrinsic birefringences δn_X (broken curve) and $-\delta n_A$ (chain curve). (*a*) λ = 547 nm. Inset: enlargement of the region around $T \simeq 3$ K. (*b*) λ = 436 nm.

magnetic fields at $\lambda = 633$ nm, where $|\delta n_X|$ is very small ($|\delta n_X| \ll 0.3 \times 10^{-4}$) and according to the limit (ii) δn_A is correctly measured. In figure 5 the measured δn_{app} is compared with a calculation according to equation (14) for $(Tb_{0.45},Dy_{0.55})VO_4$ at $\lambda = 547$ nm (figure 5(*a*)) and $\lambda = 436$ nm (figure 5(*b*)). The observed oscillation for $\lambda = 547$ nm has the same reason as discussed in connection with figure 3. Because of the greater intrinsic $|\delta n_X|$ for $\lambda = 436$ nm (figure 5(*b*)) the apparent birefringence δn_{app} approaches the intrinsic δn_X at a lower temperature already than for $\lambda = 547$ nm (figure 5(*a*)).

5. Summary

The measured apparent birefringence in the monoclinic phase of the mixed Jahn–Teller system $(Tb_x,Dy_{1-x})VO_4$ could be explained by the superposition of the intrinsic birefringences δn_A and δn_X corresponding to the distortion types Γ_4^+ and Γ_3^+. The simultaneous existence of these two birefringences affects in a non-trivial manner the measured birefringence in the experimental arrangement used. It is shown that, apart from the direct superposition of the Γ_3^+ and Γ_4^+ distortion types, no other effect acts on the birefringence. Especially the two distortions do not affect each other.

References

[1] Hess G, Dammann M, Kahle H G, Kasten A, Seifert C and Vögtlin K 1989 *J. Phys.: Condens. Matter* **2** 1073
[2] Hess G 1989 *J. Phys.: Condens. Matter* **2** 1097
[3] Nye J F 1985 *Physical Properties of Crystals* (Oxford: Clarendon)
[4] Landau L D and Lifshitz E M 1960 *Electrodynamics of Continuous Media* (Oxford: Pergamon)
[5] Koňák Č, Smutný F, Březina B and Budik L 1978 *Ferroelectrics* **21** 361–3
[6] Bismayer U, Salje E, Glazer A M and Cosier J 1986 *Phase Transitions* **6** 129–51
[7] Holzapfel W and Riss U 1987 *Appl. Opt.* **26** 145–53
[8] Jones R C 1941 *J. Opt. Soc. Am.* **31** 488–503